Skin Sea Surface Temperature schemes in coupled ocean-atmosphere modeling: the impact of chlorophyll-interactive e-folding depth.

Vincenzo de Toma[2], Daniele Ciani[1], Yassmin Hesham Essa[1,3,4], Chunxue Yang[1], Vincenzo Artale[1], Andrea Pisano[1], Davide Cavaliere[1], Rosalia Santoleri[1], and Andrea Storto[1]

[1] CNR-ISMAR, Consiglio Nazionale delle Ricerche, Istituto di Scienze Marine, via Fosso del Cavaliere 100, 00133 Rome, Italy.
[2] CNR-ISMAR, Consiglio Nazionale delle Ricerche, Istituto di Scienze Marine, Calata Porta Di Massa - Porto Di Napoli 80, 80133 Naples, Italy.
[3] GUF-IAU, Goethe University Frankfurt, Institut fuer Atmosphaere und Umwelt, Frankfurt, Germany
[4] ARC-CLAC, Agricultural Research Center, Central Laboratory for Agricultural Climate, Giza, Egypt

Correspondence to: Vincenzo de Toma (vincenzo.detoma@cnr.it)

Abstract. In this paper, we explore different prognostic methods to account for skin sea surface temperature diurnal variations in a coupled ocean-atmosphere regional model of the Mediterranean Sea. Our aim is to characterize the sensitivity of the considered methods with respect to the underlying assumption of how the solar radiation shapes the warm layer of the ocean. All existing prognostic methods truncate solar transmission coefficient at a warm layer reference depth which is constant in space and time; instead, we implement a new scheme where this latter is estimated from a chlorophyll dataset as the e-folding depth of solar transmission, therefore allowing it to vary in space and time depending on seawater's transparency conditions. Comparison against satellite data shows that our new scheme, compared to the one already implemented within the ocean model, improves the spatially averaged diurnal signal, especially during winter, and the seasonally averaged one in spring, and autumn, while showing a monthly, basin-wide averaged bias smaller than 0.1 K year-round. In April, when most of the drifters' measurements are available, the new scheme mitigates the bias during nighttime, keeping it positive but smaller than 0.12 K during the rest of the monthly-averaged day. The new scheme implemented within the ocean model improves the old one by about 0.1 K, particularly during June. All the methods considered here showed differences with respect to objectively analyzed profiles confined between 0.5 K during winter and 1 K in summer for both the eastern and the western Mediterranean regions, especially over the uppermost 60 m. The new scheme reduces the RMSE on the top 15 m in the central Mediterranean for summertime months compared to the scheme already implemented within the ocean model. Overall, the surface net total heat flux shows that the use of a skin SST parametrization brings the budget about 1.5 W/m^2 closer to zero on an annual basis, despite all simulations showing an annual net heat loss from the ocean to the atmosphere. Our "chlorophyll-interactive" method proved to be an effective enhancement of existing methods, its strength relying on an improved physical consistency with the solar extinction implemented in the ocean component.

1 Introduction

Air-sea fluxes govern the energy exchange at the ocean-atmosphere interface. A reliable representation of the Sea Surface Temperature (SST) diurnal cycle, i.e. the typical SST oscillation/excursion between night and day mainly due to solar heating, is crucial to accurately estimate air-sea heat fluxes (Kawai and Wada, 2007, Soloviev and Lukas, 2013), whose direct measurement is very difficult. Indeed, diurnal warming events can often exceed 5 K depending on weather conditions (Soloviev and Lukas, 1997) and geographical location, typically at tropical and mid-latitudes but also occasionally at high latitudes (Karagali and Høyer, 2013). Large diurnal warming events can lead to changes in air-sea heat flux locally reaching up to $60 W/m^2$ (Fairall et al., 1996, Ward, 2006, Kawai and Wada, 2007, Marullo et al., 2010, Marullo et al., 2016) on a variety of scales, ranging from the short regional ocean weather ones to large seasonal or long-term ones.

Therefore, there is a wide interest in the development of models to accurately reconstruct SST diurnal variations in order to improve the representation of air-sea energy exchanges, especially, but not solely, within the coupled ocean-atmosphere modeling framework (Penny et al., 2019).

The net energy flux across the air-sea interface results from four contributions: the net solar radiation; latent and sensible heat fluxes, and the net thermal radiation. The last three contributions depend on SST and have a direct impact in determining ocean heat uptake or dynamical processes such as deep-water formation (Chen and Houze Jr., 1997). Ideally, the most accurate flux estimate would imply the knowledge of the temperature right at the atmosphere-ocean separation interface. From an observational point of view, the skin SST is the temperature immediately adjacent to the ocean surface (~10-20 microns depth) that is measurable, typically from infrared radiometers, and thus a key parameter to understand heat flux exchange (Minnet et al., 2019). Indeed, following what is measurable by current sensors, the GHRSST-PP (i.e. the Global ocean data assimilation experiment High Resolution SST Pilot Project) introduced the distinction between skin, sub-skin, depth, and foundation SST (Donlon et al., 2007), which can be respectively regarded as successive, better-to-worse approximations to the ideal target, i.e. SST right at the interface, which is actually impossible to measure. However, in most of the widely used ocean models and configurations, the too-coarse vertical resolution does not allow to direct modeling skin SST (the first model layer being only around 0.5 - 1 meter thick, e. g. the ocean model NEMO – see the sketch in figure 1). Therefore, one must use schemes to reconstruct skin SST variations. Sadly, the only thing one can be sure about is that in general no model will be able to perfectly reproduce skin SST diurnal variations, and there are different ways to approach this challenging problem, each one still with its own limitations (see Kawai and Wada, 2007 and references therein). Simplified approaches widely employed in ocean and atmosphere state-of-the-art models parameterize the skin SST dynamics via the distinction of two main effects: the cool skin and the warm layer. Due to its interactions with the atmosphere, the temperature right at the interface of separation is supposed to be almost anywhere and anytime lower than the temperature of the waters infinitesimally close to it, resulting in the ocean being covered with a thin cool skin layer. One of the very first and simpler models assumes this cool skin temperature difference as proportional to the ratio between heat fluxes and kinematic stress (Saunders, 1967), via the Saunders' constant.

The cool skin effect is very important in obtaining accurate estimates of the latent and sensible heat flux, especially because its consideration modifies specific humidity at the ocean surface, which is one of the factors in the bulk formula. Indeed, latent and sensible heat fluxes are defined as the heat transfer across the ocean/atmosphere interface due to turbulent air motions (the former including the one resulting from condensation or evaporation). For example, a recent study in the South China Sea showed that during nighttime the cool skin temperature difference is around 1 K, and there's currently a large uncertainty in the Saunders' constant (Zhang et al., 2021). A warm layer (in which diurnal warming effectively takes place) develops below this cool skin, and its extent reaches a depth at which the penetration of solar radiation can be neglected (usually fixed to 3m by most existing parameterizations – see section 3.3 for more details). Diurnal warm layer anomalies (which can sometimes exceed 3K) can potentially impact both the atmosphere and ocean mean state on a variety of spatial (ranging from regional, basin-wide to global ones) and temporal scales (relevant for weather or seasonal forecast to long-term climatic trends) (Donlon et al., 2007). The skin SST diurnal warming amplitude increases under low surface winds (smaller than 2 m/s) and intense solar radiation (higher than typical daily peaks, around 900 W/m^2) conditions, smaller in winter and at the poles than in summer and in the tropics. The accuracy of skin SST models, and therefore their ability to reconstruct skin SST diurnal variations is crucial especially in heat budget closure problems, which are still a subject of active debate especially in climate change hot spot regions such as the Mediterranean domain (see Marullo et al., 2021 and references therein). Skin SST schemes are also crucial for assimilating daytime SST data from satellite sensors (Penny et al., 2019; Storto and Oddo, 2019, Jansen et al., 2019), with obvious impact on the accuracy of numerical weather and ocean predictions; a correct account of skin SST diurnal variations in turn is crucial for flux calculations, which is already a very delicate problem also from an instrumental point of view.

Within these prognostic schemes, seawater's transparency conditions (e.g., estimated using chlorophyll concentration) have great implications in the way solar radiation is absorbed within the ocean's uppermost layer (Morel and Antoine 1994). Ohlmann et al. 2000 quantified with the help of radiative transfer calculations effects of physical and biological processes on solar radiation transmission, classifying as main factors chlorophyll concentration, cloud cover and solar zenith angle. Ohlmann and Siegel 2000 and Lee et al. 2005 are further examples of how radiative transfer models are used to develop solar transmission parameterization which is fit to the sum of exponentials (the number of terms in the sum depending on the variable which has been considered). To the best of our knowledge, these ideas have not been implemented nor tested within the prognostic scheme for skin SST present in the ocean model NEMO, which just relies on chlorophyll-calibrated coefficients through Gentemann et al 2009.

Our main aim here is therefore to improve existing skin SST prognostic schemes, investigating the impact of variable seawater's transparency conditions in modeling solar radiation extinction in the upper ocean. The use of chlorophyll concentration as a proxy for seawater's transparency is not new. In fact, given its covariance with Secchi disk depth (estimated from reflectance at various wavelength), it has been often applied by the ocean color community to study the dynamics of oligotrophic gyres (Leonelli et al., 2022 and references therein). The paper is structured as follows: after this introduction, we describe the data and coupled modeling

system in section 2. The mathematical context in which we developed our new method, whose novelty stands in allowing the warm layer's extent to vary in space and time according to a chlorophyll-concentration climatology follows in section 3. In section 4 we present results, discussing them and drawing conclusions in section 5.

2   Data and Modeling System

We describe here the data and the coupled regional modeling system used in this study. Our description here is functional to the scope of this paper, and far from a complete depiction of each dataset. We refer readers to the documentation and relevant literature for detailed information on each dataset and model.

2.1   Operational MED DOISST within CMEMS

The MEDiterranean Diurnal Optimally Interpolated Sea Surface Temperature (MED DOISST) product, operationally distributed and freely available within the Copernicus Marine Environmental Service (CMEMS) provides gap-free (L4) hourly mean maps of sub-skin SST at $1/16^o$ horizontal resolution over the Mediterranean domain, covering from 2019 to present. Sub-skin SST is defined as the temperature at the base of the cool skin layer, typically sensed by microwave radiometers, and representative of a depth of few millimeters from the ocean's surface (Minnet et al., 2019).

This product combines satellite data acquired from the Spinning Enhanced Visible and InfraRed Imager (SEVIRI) and model data from the Mediterranean Forecasting System (MedFS), respectively used as observations and first guess for an optimal interpolation, giving a L4 field representative of subskin SST (see Pisano et al., 2022 and references therein). In all diagnostics involving these data (and presented in the following sections), regions where the percentage of valid SEVIRI measurements is lower than 50% have been masked out both in CMEMS MED DOISST and our experiments.

2.2   iQuam in-situ data

SST from drifter data were used for validation purposes and acquired from the iQuam (In situ SST Quality Monitor) archive (Xu and Ignatov, 2014). The iQuam provides high-quality and quality controlled (QC) in-situ SST data collected from various platforms, such as drifters, Argo Floats, ships, tropical and coastal moored buoys. iQuam SST data are also provided along with quality level flags ranging from 0 to 5, with 5 corresponding to the highest quality level (Xu and Ignatov, 2014). For this study, SST with quality level equal five were selected from drifters only, since they provide the temperature measurement closest to the surface (compared to the other available instruments), ranging between 20-30cm (depending on the drifter type).

Additionally, we interpolated model outputs on drifters' location in time and space. Table S1 outlines the number of available measurements for each given month and hour of the day. A total number of 555919 records

were available after the quality flag and platform selection, with the month of April being the most populated one, with 222996 measurements, and 10361 measurements at 9:00 am.

2.3   EN4 objective analysis

EN4, the quality controlled subsurface ocean temperature and salinity profiles and objective analyses, were used to assess the impact on the temperature vertical profiles. To facilitate the comparison, we made use of the objective analyses after bias corrections of Expendable Bathythermograph (XBT) calibrations (Gouretski and Reseghetti, 2010, Gouretski and Cheng, 2020), which give a gridded version of the dataset on a 1-degree regular grid. In the comparison, model outputs were interpolated on this grid.

2.4   Mediterranean Chlorophyll concentration

Chlorophyll data were used to estimate e-folding depths' seasonality (see Methods, Section 3). These data are a daily interpolation at 0.3 km horizontal resolution over the Mediterranean domain, and result from a merging between multiple sensors (MERIS - MEdium Resolution Imaging Spectrometer from ESA, SeaWiFS - Sea-viewing Wide Field-of-view Sensor and MODIS - Moderate Resolution Imaging Spectroradiometer from NASA, VIIRS - Visible Infrared Imager Radiometer Suite from NOAA, and most recently the Copernicus Sentinel 3A OLCI - Ocean and Land Colour Instrument), as detailed in the product description (see Volpe et al., 2019 and references therein for further details).

2.5   ECMWF Atmospheric Reanalysis - ERA5

We used heat fluxes (net solar radiation, latent and sensible heat fluxes, net thermal radiation) from ERA5 at $0.25°$ horizontal and hourly temporal resolution (Hersbach et al., 2020) as reference for comparing performances across simulations with different skin SST schemes. Despite their possible biases in air-sea fluxes, atmospheric reanalyses today are still widely thought to provide the best gap-free and dynamically consistent reconstructions of the atmosphere system (Valdivieso et al., 2017, Storto et al., 2019).

2.6   Mixed Layer Depth 1969-2013 Climatology

Data from a mixed layer depth (MLD) climatology was used to test to what extent our modified scheme correctly represents the seasonality of the mixed layer.
This monthly gridded climatology was produced using MBT, XBT, Profiling floats, Gliders, and ship-based CTD (Conductivity, Temperature, Depth) data from different databases and carried out in the Mediterranean Sea between 1969 and 2013. As for the model outputs, MLD is calculated with a $\Delta T = 0.1°C$ criterion relative to 10m reference level on individual profiles (Houpert et al., 2015a, Houpert et al., 2015b).

 2.7   ISMAR Mediterranean Earth System Model (MESMAR)

180   MESMAR is a newly developed coupled regional modeling framework for the Mediterranean region (Storto
181   et al., 2023). MESMAR includes the following components:

- 182   • the ocean model: NEMO v4.0.7, with horizontal resolution of about 7 *km*, 72 unevenly spaced vertical
- 183   levels (the first and the last levels being respectively about 0.5m and 200m thick) and a timestep of 7.5
- 184   minutes (NEMO System Team, 2019);

- 185   • the atmosphere model: WRF v4.3.3, with 41 vertical hybrid levels and horizontal resolution of about 15
- 186   *km*, covering the European branch of the international Coordinated Downscaling Experiment (EURO-
- 187   CORDEX) domain, and a timestep of 1 minute (Skamarock et al., 2019);

- 188   • an interactive runoff model: HD v5.0.1, with a timestep of 30 minutes and 1/12° degree horizontal
- 189   resolution over Europe (Hagemann et al., 2020);

- 190   • the coupler: OASIS3-MCT, coupling the three models with a coupling frequency of 30 minutes, and
- 191   using the SCRIP library to interpolate fields between different model grids (Craig et al., 2017);

192   We report in figure 2 a graphical summary of different grids. Further details of its implementation, tuning, and
193   performances are described in (Storto et al., 2023).
194

3   Methods

196   Many schemes to reconstruct the skin SST diurnal variations rely on the existence of a cool skin and a warm
197   layer, respectively in the upper micrometers and few meters of the ocean, whose dynamics strongly depends on
198   wind conditions and solar radiation extinction within the upper ocean. To explain the rationale behind the
199   developments in our new method, we need to recap here some elements of this theory, which is mostly based
200   on Zeng and Beljaars, 2005 (named ZB05 hereafter) work.
201   We start from the one-dimensional heat transfer equation in the ocean:

$$\frac{\partial T}{\partial t} = \frac{\partial}{\partial z}\left(K_w + k_w\right)\frac{\partial T}{\partial z} + \frac{1}{\rho_w c_w}\frac{\partial R}{\partial z}$$

(1)

203   in which the subscript w refers to water properties, T is seawater temperature (K), K_w ($m^2 s^{-1}$) is the turbulent
204   diffusion coefficient, k_w ($m^2 s^{-1}$) is the molecular thermal conductivity, ρ_w ($Kg\ m^{-3}$), c_w ($J\ Kg^{-1} K^{-1}$) are respectively
205   seawater density and heat capacity per unit volume, R ($W\ m^{-2}$) is the net solar radiation flux, defined as positive
206   downward.

3.1 Cool Skin

We assume that there exists an oceanic molecular sublayer of depth δ, where K_w is negligible, and temperature can be assumed constant in time, since it is always cooler than temperature of the underlying seawater (Donlon et al., 2007, Zeng and Beljaars, 2005). Then integration of eqn. (1) gives, $\forall z \in [0, -\delta]$

$$k_w \frac{\partial T}{\partial z} + \frac{1}{\rho_w c_w}[R(z) - R_s] - k_w \cancel{\frac{\partial^2 T}{\partial z^2}}^{\mathcal{O}(z^2)} = const, \tag{2}$$

where R_s is the net solar radiation at the surface (constant, open-ocean albedo, since the Mediterranean Sea is an ice-free basin), assuming this constant to be the top boundary condition at $z = 0$:

$$\rho_w c_w k_w \frac{\partial T}{\partial z}\Big|_{z=0} = Q = LH + SH + LW, \tag{3}$$

in which *LH, SH, LW* are respectively the surface fluxes of latent, sensible heat and net long wave radiation.

Thus, eqn. (2) can be rewritten as

$$\rho_w c_w k_w \frac{\partial T}{\partial z} = Q + R_s - R(z). \tag{4}$$

Making a further integration we get the cool skin temperature difference:

$$T_s - T_{-\delta} = \frac{\delta}{\rho_w c_w k_w}(Q + f_s R_s), \tag{5}$$

where T_s and $T_{-\delta}$ are respectively the temperature at the upper (air-sea interface) and lower limits of the cool skin layer, while f_s is the fraction of solar radiation absorbed in this layer:

$$f_s = \frac{1}{\delta} \int_{-\delta}^{0} \left(1 - \frac{R(z)}{R_s}\right) dz,$$

which depends on the way radiation gets absorbed within the cool skin. Being time-independent, the cool skin temperature difference is a diagnostic variable in the scheme.

Eq. (5) is analogous to Saunders' model. Indeed, Saunders, 1967 was one of the first to construct a theory for the ocean "cool skin" effect, i.e. the observed temperature at the air-sea interface is generally cooler than the temperature of the water at about 10 cm depth, especially during nighttime. This effect takes place mainly because of the transfer of energy between the ocean and the atmosphere, realized via heat loss and momentum transfers (wind stress). In a nutshell, at the end of its derivation (Saunders, 1967), he obtains the following expression for the temperature difference across the cool skin, ΔT_c (K):

$$\Delta T_c = \lambda \frac{Q \nu_w}{k_w (\tau/\rho_w)^{1/2}}, \tag{6}$$

234 where λ is the Saunders' proportionality constant, Q $(W\,m^{-2})$ has already been defined above, τ/ρ_w $(m^2\,s^{-2})$ is the

235 kinematic stress (ratio between wind stress module and seawater density), and $v_w,(m^2 s^{-1})$ k_w $(m^2 s^{-1})$ are

236 respectively the kinematic viscosity and thermal conductivity of seawater. Saunders' formulation was originally

237 conceived for low, nonzero wind conditions and neglecting the effect of solar radiation (although recognized

238 its role and added a discussion on how to account for it in the model only at the end of his paper). As noticed

239 by Fairall et al. 1996, Artale et al., 2002 (named A02 hereafter), with a constant λ, eqn. (6) becomes problematic

240 in limiting cases of low and very high wind speeds (greater than $7\ m/s$), because the wind stress in the

241 denominator limits its validity. Thus, A02 proposed to include a wind dependence in Saunders' constant, in

242 order to still have a finite, nonzero cool skin to bulk temperature difference even when the wind speed goes to

243 zero or becomes very high. This scheme has proven to have good performances compared to other schemes

244 also on a mooring site in the Pacific Ocean (Tu and Tsuang, 2005).

245

246 **3.2 Warm Layer**

247 Below the skin layer, turbulent transfer is much more effective, and k_w can be neglected in favor of K_w.

248 Integrating eqn. (1) within the $[-d,\ -\delta]$ layer, we get:

$$\frac{\partial}{\partial t}\int_{-d}^{-\delta} T\ dz = \frac{Q + R_s - R(-d)}{\rho_w c_w} - K_w \frac{\partial T}{\partial z}\bigg|_{z=-d}\,,$$

249 (7)

250 where d is a reference depth which can be assumed as the depth at which the diurnal

251 cycle can be omitted.

252 The turbulent diffusion coefficient can be expressed as (Large et al., 1994):

$$K_w = k u_{*w}\,(-z)\,/\phi_t\left(\frac{-z}{L}\right),$$

253 (8)

254 in which $k = 0.4$ is the Von Karman constant, z is negative in the ocean, u_{*w} is the friction velocity in the water

255 (this being the air friction velocity multiplied by the square root of air to sea density ratio), and the stability

256 function ϕ_t discriminates between a stable and an unstable regime, depending on the sign of its argument, which

257 is the ratio of the vertical coordinate to the Monin Obukhov length L: positive for the stable and negative for

258 the unstable one. Assuming z to be negative in the ocean, the change of sign entirely depends on the Monin

259 Obukhov length, which is a length characterizing the prevalence of buoyancy variations induced turbulence

260 over the one generated by wind shear effects. This in turn is strongly dependent on the sign of the net heat flux

261 Q. If $Q>0$, i.e. the ocean gains heat from the atmosphere, and we have the stable regime: the diffusion

262 coefficients decrease with increasing depth, favoring the downward heat transfer within the water column. The

263 opposite case, which favors transfer of heat from the ocean to the atmosphere, can be modeled in different ways

264 (see While et al., 2017 and references therein).

265 Assuming a temperature dependence, for $d \gg \delta$ of the form

$$T = T_{-\delta} - \left[\frac{z+\delta}{-d+\delta}\right]^{\nu}(T_{-\delta} - T_{-d})\,,\qquad \nu \text{ empirical parameter}$$

266 (9)

267   eqn. (7) simplifies to

$$\frac{\partial}{\partial t}\left(T_{-\delta} - T_{-d}\right) = \frac{Q + R_s - R(-d)}{d\rho_w c_w}\frac{\nu + 1}{\nu} - \frac{(\nu + 1)ku_{*w}}{d\phi_t\left(d/L\right)}\left(T_{-\delta} - T_{-d}\right)$$

268   (10)

269   In ZB05 scheme (Zeng and Beljaars, 2005), eqs. (5, 10) are the coupled equations for the cool skin (diagnostic

270   part) and warm layer (prognostic part) respectively. Being time dependent, the determination of the warm layer

271   temperature difference at time t requires the knowledge of the one at the previous time step, and thus is the

272   prognostic variable in the scheme. Assumptions on the fraction of solar radiation within the warm layer and the

273   cool skin depth usually follow Fairall et al., 1996 parameterization, whose detail are given in the Supplementary

274   Material section.

275

276   **3.3   Solar transmission expression**

277   The expression of the solar transmission in Zeng and Beljaars, 2005 is

$$\frac{R(-d)}{R_s} = \sum_{i=1}^{3} a_i e^{-db_i}, \qquad \begin{array}{l}(a_1, a_2, a_3) = (0.28, 0.27, 0.45), \\[6pt] (b_1, b_2, b_3) = (71.5, 2.8, 0.07)m^{-1},\end{array}$$

279   following Soloviev formulation (Soloviev, 1982) (S82 in the following), which is very widely used in

280   atmosphere models (such as WRF, Skamarock et al., 2019).

281

282   So far this is not the only possibility: a formulation with 61 coefficients has been developed by Jerlov, 1968,

283   which is based on different water types classified based on chlorophyll concentration and particulates, for light

284   in the visible spectrum.

285

286   Formulations with 9 coefficients (reported in Table 2) have been proposed to include such effects: for example

287   Soloviev and Schlussel, 1996 use a different coefficient for the first term depending on Jerlov's optical water

288   type, while Gentemann et al., 2009 include solar angle in the parameterization, keeping the value of the first

289   coefficient as in the case of pure-water. Without knowing what the Jerlov water type is, what is currently

290   implemented in NEMO is to take b_1 as the average between coefficients for I, IA, IB, II and III Jerlov's optical

291   water types. This formulation is widely employed in ocean models (such as in the optional skin SST routine of

292   NEMO, see While et al., 2017), with the reference depth d fixed to 3 m. So, the solar transmission follows as:

$$\frac{R(-d)}{R_s} = \sum_{i=1}^{9} a_i e^{-db_i}.$$

293   (13)

294   Ideally, one would like to have a reference depth representative of the one at which the transmission of solar

295   radiation is negligible, and if we take it as the depth at which transmission drops to $1/e$ from its surface value,

296   we get a value which can be different from $d = 3$ m, as we can see from figure 3a. Allowing for a realistic time

297   and space varying value of d represents the main novelty of our work.

298

299 From this viewpoint, choosing a value of $d = 3\ m$ while using the solar extinction formulation as in Soloviev,

300 1982 or Soloviev and Schlussel, 1996 would lead to underestimating the penetration of solar radiation into the

301 warm layer. Another possibility, which constitutes our modification to the scheme already implemented in

302 NEMO, is to reconstruct a chlorophyll profile from its surface values following what is already implemented

303 in the NEMO module for radiation calculations (Jerlov, 1968, Morel et al., 1989, Lengaigne et al., 2007), and

304 employ an R-G-B+Chl-a scheme to calculate radiation as a function of depth. Then, from eqn. (13) with only

305 4 terms (one for chlorophyll, and three for R-G-B, expressed in lookup tables), one can numerically derive the

306 warm layer reference depth as the e-folding depth of the light extinction profile (see Fortran source files in the

307 Zenodo repository, de Toma (2024))..

308

309 This would give a constant transmission throughout the basin, but with a spatially and temporally varying e-

310 folding depth and defines our new prognostic scheme for skin SST warm layer calculation, thus embedding in

311 it the ocean color information coming from Chl-a. Everything else is left unchanged, both the refinements of

312 Takaya et al., 2010, which include the effect of Langmuir circulation and a modification of the Monin-Obukhov

313 similarity function under stable conditions (T10 hereafter), and the A02 model for cool skin, which has been

314 demonstrated to improve the scheme respectively under wavy and windy conditions.

315 ### 3.3.1   E-folding depth estimates

316 Mediterranean Chlorophyll climatology data (see section 2.4) were re-gridded onto a 0.25 ° regular

317 longitude/latitude grid, and tabulated coefficients within NEMO were used to retrieve the transmission,

318 accounting for chlorophyll variations. E-folding depths then can be estimated as the depth at which transmission

319 drops to 1/e from its surface value. It can be noticed from figure 3b that also the e-folding depth varies with

320 seasonality, with typical values ranging from about 3 to 4.5 meters. This is the central point of our modification

321 to the prognostic scheme. In our setup we extracted pixelwise and at each time step of the NEMO model the e-

322 folding depth used within the prognostic scheme.

323 ### 3.4   Overview of the simulations performed.

324 With the coupled ocean-atmosphere regional system we performed a set of four simulations, forced by

325 ERA5 in the atmosphere and ORAS5 (Zuo et al., 2018) in the ocean and covering three years (from 2019 to

326 2021), with hourly outputs (a synthesis is provided in Table 1). In cases where a skin SST scheme is active, we

327 substitute the SST, i.e. temperature on the first NEMO level, with the skin SST coming out from the scheme:

328 1. a control run, in which no skin SST prognostic scheme is activated, therefore the diurnal SST variations

329 in the uppermost ocean layer (0.5 m thick) only come from the variability represented by the ocean model

330 at about 0.5 m of depth, considering also the 0.5 hours frequency of the coupling. We will refer to this

331 experiment in the following as *ctrlnoskin*;

2. a run in which the ZB05 scheme in WRF (Zeng and Beljaars, 2005) is active – we shall refer to this case in the following as *wrfskin*;

3. a run in which the existing scheme within NEMO, which employ the 9-coefficient parameterization for light extinction coefficients (Gentemann et al., 2009 – G09 hereafter), the scheme for the cool skin as modified in A02, and refinements of the stability function, in the warm layer formulation as in T10 – we shall refer to this as the *nemoskwrite* case;

4. a fourth simulation in which we modified the reference depth for the basis of the warm layer from $z = 3$ m, to an e-folding depth (i.e. the depth at which radiation gets diminished by $1/e$ from its surface value), which is allowed to vary temporally and spatially because it is estimated from R-G-B light extinction coefficients and chlorophyll concentration (see section 3). We will refer to it as *modradnemo*, being the experiment where our modification to the skin SST scheme is implemented and tested.

The reason behind the choice of the above mentioned period of three years 2019-2021 is twofold: firstly, it allows a validation against all the measurements from different data sources (satellite, drifters and objectively analyzed profiles), and secondly, it is a good trade-off between the needs of keeping a reasonable computational load, data volume for the analysis, and guarantees a minimal robustness of our finding, compared to a simulation which covers just one year. However, we do not discard the possibility to extend the time coverage in our plans for future works.

4   Results

In this section, we present skill scores against satellite, drifters and temperature profiles data (see section 2) from the set of the simulations performed, aimed at characterizing the impacts of our modified skin SST scheme. Since we are mainly acting to improve skin SST diurnal variations reconstruction in the ocean component, the main focus is on the difference between the nemoskwrite and modradnemo, while the ctrlnoskin and wrfskin ones are included as further reference elements (the latter being not directly comparable because the atmospheric model sees the ocean foundation SST and employ the scheme just to diagnose the skinSST).

4.1   Comparison with CMEMS MED DOISST

We calculated the mean diurnal warming amplitude in each season as the seasonally averaged diurnal warming amplitudes (diurnal warming amplitude being defined for each day as the difference between daytime maximum and nighttime minimum of SST), which can be cast into the following equation:

$$\langle \text{DWA} \rangle_{\text{seas}} = \frac{1}{N_{\text{seas}}} \sum_{i=1}^{N_{\text{seas}}} \left\{ \max_{h_i \in [10:00, 18:00]} \text{SST}\,(h_i) - \min_{h_i \in [00:00, 06:00]} \text{SST}\,(h_i) \right\},$$

(14)

362   where seas = DJF, JJA, MAM, SON is the given season, N_{seas} is the number of days in that particular season

363   and h_i is the local time in hours for any given day.

364   Seasonally averaged diurnal warming amplitudes are shown in figure 4. On average, the maximum amplitude

365   is reached in summer, with the wrfskin simulation peaking at about 3 *K*, thus overestimating the mean diurnal

366   cycle compared to CMEMS MED DOISST (the monthly biases with respect to CMEMS foundation SST both

367   in the western and the eastern part of the Mediterranean Sea stay below 1 *K* year-round for all of the simulations

368   performed – see figure S1 in Supplementary Materials). The nemoskwrite simulation yields a pattern very

369   similar to CMEMS MED DOISST in summer, but underestimates the signal in the remaining seasons. Outside

370   the Summer season, our modifications yield a slight improvement (see modradnemo, last row of figure 4). As

371   expected, the control run in which no skin SST method is active, generally underestimates the diurnal signal

372   everywhere. Compared to nemoskwrite, the modradnemo simulation improves JJA mean diurnal warming

373   amplitude, especially over the Southern Mediterranean Sea, while in central and Northern part of the basin

374   tends to overestimate the signal by about 0.5 K with respect to CMEMS-DOI data. Furthermore, a general

375   underestimation is present also in DJF, with the modradnemo simulation showing the smallest differences with

376   respect to CMEMS-DOI data.

377   The spatial average over the whole Mediterranean domain is shown in figure 5, confirming the general

378   underestimation of the control run and the overestimation of the wrfskin and modradnemo in all seasons except

379   winter.

380   Computing spatial averages highlights that modradnemo slightly improves the mean diurnal warming

381   amplitude signal during wintertime, while in all the other seasons the best agreement is gained by using the

382   nemoskwrite setup (ZB05 with T10 and A02 modifications), at least according to the verification against

383   CMEMS MED DOISST.

384   On a monthly timescale, figure 6 confirms that the control simulation tends generally to have a negative bias

385   of the diurnal amplitude, for the whole simulated period. The wrfskin (ZB05 scheme) shows a warm bias during

386   summertime months, shown just as a reference. The comparison between nemoskwrite (ZB05+A02+T10) and

387   modradnemo (chl e-folding depth) shows improvement of our scheme (modradnemo) over the old one

388   (nemoskwrite) especially in May, but not in April, June, July, August and September, despite in the rest of the

389   period the amplitude of the bias is slightly reduced.

390   **4.2   Comparison with iQuam Star HR-Drifters**

391   The bias with respect to drifter measurements averaged over drifters positions as a function of the month

392   and time of the day is shown in figure 7. All the schemes present a systematic cool bias in autumn (SON) for

393   most of the hours of the day. During April and June, the modradnemo simulation significantly reduced the

warm bias with respect to observations, compared to the nemoskwrite case, keeping it however generally positive. This is quite reasonable, since drifters measurement can be thought representative of a depth which can also be below the subskin level (typically of the order of some centimeters). Consistently with figure 6, the wrfskin has a larger positive bias than modradnemo in June.

Further, as shown by figure 8, the bias between CMEMS MED DOISST and drifters is generally positive anytime except in late spring/summer and autumn during nighttime. This pattern arises because of the composite effect of having a temperature representative of the subskin level where and when there are data from radiometers, and a temperature of about $1\,m$ depth from the MEDFS system as first guess of the optimal interpolation over cloudy regions (Pisano et al., 2022). However, the modified scheme significantly reduces the difference, yielding a bias closer to the one of CMEMS MED DOISST with respect to drifters, especially during April, which is the month in which the number of observations from drifters is definitely larger.

4.3 Comparison with EN4 objective analysis

Bias corrected vertical profiles gathered in an objective analysis were used to assess differences across schemes along the water column. To summarize we report here only a macro subdivision into the eastern and the western Mediterranean Sea, respectively in figures 9, 10. Model outputs were remapped on the same vertical and horizontal grid. Looking at the mean profile averaged over all grid points in the given area, the agreement is better for all simulations during summertime months, both for the eastern and the western region (see figs. 9c, 10c), showing in particular that the modradnemo simulation outperforms the nemoskwrite one. This is also true for the wintertime season in the eastern Mediterranean (see fig.9b). On the other hand, in the western Mediterranean all simulations tend to overestimate the signal, with our modified scheme doing a better job with respect to the nemoskwrite case, with an average profile which is about 0.4°C closer to the EN4 profile. However, below about $80\,m$ depth differences across schemes vanish.

Looking in more detail at the RMSE on the top $15\,m$ depth between each simulation and EN4 as a function of the month and more detailed region subdomains shown in figure 11a, we can see how in general all simulations present the same pattern for the region outside of Gibraltar Strait, which can be thought an effect related to the presence of the relaxation to horizontal boundary conditions, while for all the remaining regions and months the control run, the wrfskin and the modradnemo present a similar pattern, with the modradnemo reducing the RMSE in most of the regions and for most of the months, especially with respect to nemoskwrite, and this is particularly true over the central Mediterranean Sea, in regions like Thyrrenian and Adriatic Seas.

4.4 Heat fluxes and vertical propagation

In this section we aim to characterize the differences of each scheme with respect to the control simulation. We do this by specifically looking at the seasonality of Mixed Layer Depth (MLD), vertical profiles of

temperature in specific months and regions, and via the comparison of the net surface heat fluxes over the whole Mediterranean Sea.

Compared to the Mixed Layer Depth climatology from 1969 to 2013 (Houpert et al., 2015a, Houpert et al., 2015b, section 2.7), all of the tested schemes seem to have a similar impact on Mixed Layer Depth's seasonality, with larger differences with respect climatological values being mostly located in the Eastern Mediterranean Sea and during wintertime/spring (Figure 12). It may seem from this picture that there's not such a huge change to prefer one method over the other considered in this paper, and this may also be because of the short period simulated (2019-2021). Figure 13 show how our modified scheme allows more (less) vertical propagation of the diurnal signal during summer (winter) with respect to schemes with constant e-folding depth in all central regions of the Mediterranean domain (regions 2, 3, 4 as defined in figure 11a), when all of them are referenced to the control simulation temperature daily minimum.

Indeed, from figure 13b, we can see that when all the temperature profiles for each simulation are referenced to the ctrlnoskin daily minimum, there is a much wider diurnal warming signal for most of all the considered depths level, with modradnemo representing an intermediate situation between the wrfskin and the nemoskwrite simulation. This is probably due to the inclusion of chlorophyll-interactive variations, which allow for a better representation of the variability of the mixed layer dynamics.

Estimates of the mean Mediterranean heat exchange between ocean and atmosphere based on previous studies range from -11 to +22 W/m^2, with an evident dominance of negative estimates, i.e., heat loss from the ocean to the atmosphere (Jordà et al., 2017, Pettenuzzo et al., 2010). Some other studies suggest that the Mediterranean heat budget is close to a neutral value, -1 W/m^2 (Ruiz et al., 2008) or +1 W/m^2 (Criado et. al., 2012). Many factors can contribute to such wide variability among different estimates, such as differences in the parameterizations employed, initial and boundary conditions, and the way the physical processes, especially through the Strait of Gibraltar are modeled (Macdonalds et al., 1994, Gonzales, 2023).

As shown by table 3, all simulations on an annual basis give a negative, non-closed balance for the net surface heat flux, and modifications to include skinSST, performing very similarly one to another, bring the budget by 1.5 W/m^2 closer to zero, while ERA5 data show a positive net surface heat flux close to 5 W/m^2. However, all estimates fall into the (large uncertain) literature-based estimates. On seasonal timescales, the inclusion of skinSST diurnal variations has the following effects:

- less net heat loss to the atmosphere during wintertime with respect to the control run (wrfskin differing from the ctrlnoskin by about 6W/m^2, while nemoskwrite and modradnemo having a similar impact, with a difference of about 4W/m^2 with respect to the control run);

- in springtime, all simulations show a positive imbalance, with the highest difference with respect to the control run of about 1 W/m^2 in the modradnemo simulation;

- during summer, our modified scheme brings on average about 3 W/m^2 more than the control simulation into the basin, yielding an estimate which is closer to ERA5;

- in autumn, our scheme cools down more than the control (about 2 W/m^2), being the farthest simulation from ERA5 estimate, while traditional schemes tend to have a less negative net heat input.

All seasons except spring show larger difference with respect to ERA5 fluxes, with underestimation in summer, and overestimation during winter and autumn, resulting in a bias of about 10 W/m^2 with respect to the net heat flux annual budget in ERA5.

5   Summary and Conclusions

In this paper we studied the sensitivity of a regional coupled ocean-atmosphere-hydrological discharge regional model on the Mediterranean Sea to prognostic schemes for skin sea surface temperature. Specifically, we developed a new scheme which allows for spatial and temporal variations of the warm layer's extent according to seawater's transparency conditions. This is possible by using tabulated solar extinction coefficients already used in the ocean model, and inverting the functional form which determines how the solar radiation varies along the vertical direction to find the depth at which this latter drops to $1/e$ from its surface value.

We simulated the period 2019-2021, analyzing hourly model outputs, and comparing aggregated results with satellite, objectively analyzed and drifters data. Overall, the comparison with data shows that the new scheme improves what is already implemented in NEMO, e.g. mean diurnal warming amplitudes are closer to satellite observations in winter, spring and autumn, not being much worse than other existing schemes in summer, at least looking at maps of mean diurnal warming amplitude grouped by seasons. Looking to the typical temperature profile in both the eastern and the western Mediterranean Sea, non-negligible differences across schemes stay confined in the topmost $20m$ ($100m$) of depth during summertime (wintertime). Regionally, typical profiles are warmer than EN4 observation year-round for western regions (regions -1,1,2) especially in winter, while regions in the east show a smaller RMSE in the topmost meters for basically all the regions and months when comparing modradnemo to nemoskwrite. The Adriatic Sea has a systematically higher RMSE with respect to EN4 in all the tested methods, for the whole period considered. In the central regions, the new scheme penetrates temperature anomalies more (less) during summer (winter) months, having a less intense mean diurnal warming amplitude signal in summer, especially over the upper few meters (the converse holds for wintertime values). Therefore, with respect to the ctrlnoskin simulation, nemoskwrite shows the coldest signal, the wrskin the hottest, and our modification modradnemo constitutes the middle situation, with milder summer and winter than the control run. Our interpretation is that within modradnemo, the chl-interactive e-folding depths allow, where and when necessary, the warm layer to become a little deeper than in the already existing scheme (nemoskwrite), depending on chl-variations. For these space-time points, solar penetration is increased and so it tends to make warmer the warm layer. Therefore, future research efforts should be devoted

to the better characterization of this aspect, especially to understand if the modified vertical penetration of heat has some particular effect on the dynamics of the mixed layer (see Song and Yu, 2017 and references therein). Furthermore, testing the implementation within NEMO of more sophisticated radiative transfer models (such as the one of Ohlmann and Siegel 2000), or the development of deep learning based parameterizations are underway as future research efforts. On a long-term perspective, the method needs to be tested also in other areas and for longer periods, which can increase the results' certainty and allow for usage in investigating impacts on relevant climate large-scale phenomena, where the role of an improved diurnal warming signal could be more relevant (Bernie et al., 2007, Bernie et al., 2008). These includes phenomena and physical processes such as propagation of Marine Heat Waves (MHW) or deep water formation and deep convective events.

Code and data availability

The NEMO ocean model code (v4.0.7) is available at https://forge.ipsl.jussieu.fr/nemo/wiki.

The WRF atmospheric model code (v4.3.3) is available at https://github.com/wrf-model/WRF.

The HD hydrological discharge model (v5.1) is available at https://zenodo.org/record/5707587#.Y-0VQ3bMKUk.

The frozen version of the MESMARv1 code used in this manuscript is available at: https://doi.org/10.5281/zenodo.7898938.

CMEMS MED DOISST Data downloaded from CMEMS portal.

Chlorophyll data are freely available from CMEMS portal.

The iQuam data version of this study used is V2.1, downloaded from the National Environmental Satellite, Data, and Information Service Satellite Applications and Research NOAA NESDIS STAR portal.

Gridded analyses of EN4 profiles are distributed from the MetOffice Hadley Centre Observations (we used version 4.2.1).

ERA5 data are freely available after registration on the Climate Data Store (CDS) by Copernicus Climate Change Service (C3S).

MLD data are distributed on a 0.25 degree regular grid, and freely available from the Sea Open Scientific Data Publication SEANOE portal.

Minimal data and scripts used within the manuscript to reproduce the figures in the manuscript are available at this link:

https://zenodo.org/records/10451206

Acknowledgments. We specifically acknowledge Olivier Marti (LSCE/IPSL) and Aurore Voldoire (CNRM-CNRS) for fruitful discussion during the 6th Workshop on Coupling Technologies for ESM held from 18 to 20 January 2023 in Tolouse, and Sophie Valcke (CERFACS) for their valuable support in the use of the NEMO and WRF interfaces to the OASIS coupler. This Research is supported by the Research Program CN00000013 "National Centre for HPC, Big Data and Quantum Computing", Directorial Decree granting financing no. 1031 of 06.17.2022 from the resources of the PNRR MUR - M4C2 - Investment 1.4 - "National Centers" Notice - D.D. n. 3138 of 16 December 2021.

Author Contributions. VdT and AS conceived the study and designed the experiments to conduct, VdT Performed the simulation and data analysis, data downloading and writing of the first draft, VdT, DC, YH, CY, VA, AP, DC, RS and AS equally contributed to discuss and interpret the results, finalizing the draft.

Competing Interests. All authors declare they have no competing interests.
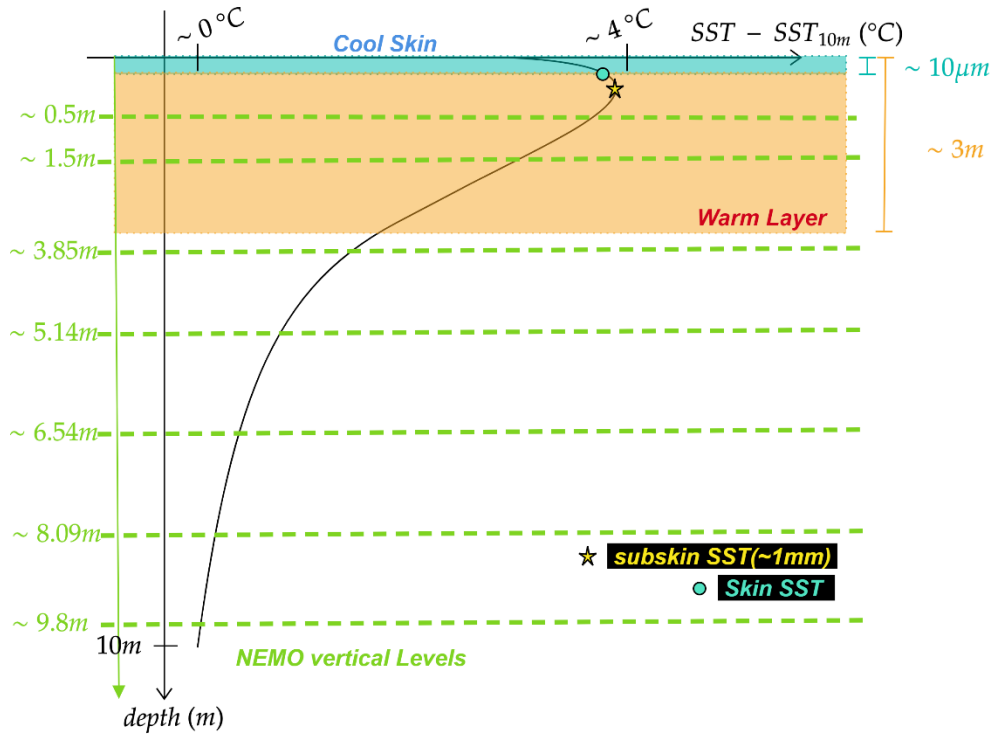
Figures

Figure 1. Sketch of the cool skin and warm layer adapted from Donlon et al., 2007. Vertical discretization of NEMO levels is shown in green (not perfectly in scale with the underlying y-axis).

562
563

564
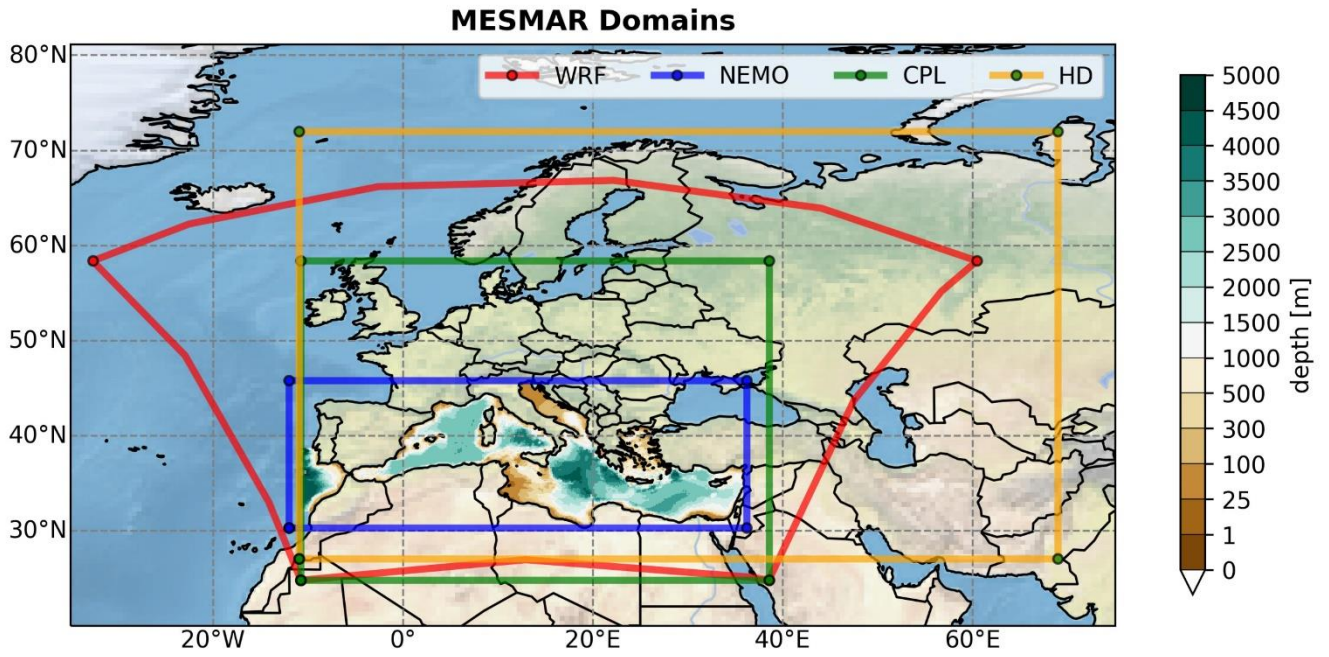
Figure 2: The modeling system domain: WRF, NEMO, HD and boundaries for the coupling mask are respectively in red, blue, orange, and green. Contour filled plot shows the ocean model bathymetry.

567
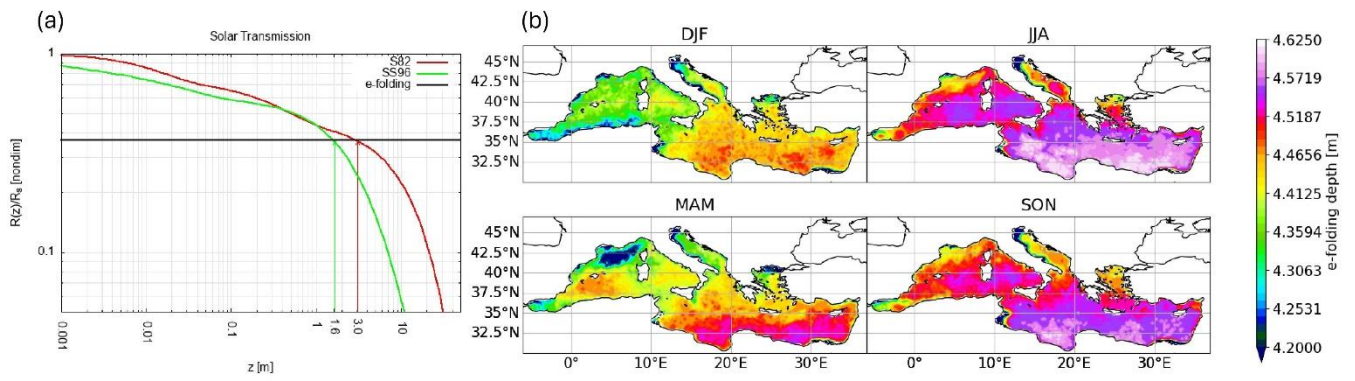
Figure 3: Panel 3a shows two different formulations frequently used for the transmission coefficient expression: the red curve shows the formulation of Soloviev, 1982, while the green curve the one defined in Soloviev and Schlussel, 1996. Panel 3b shows e-folding depth estimates from Mediterranean Chlorophyll climatology of Volpe et al., 2019: lowest values touch the 2.5 meters. Note that the x-axis range does not start from 0 to allow a logarithmic representation of the depth.
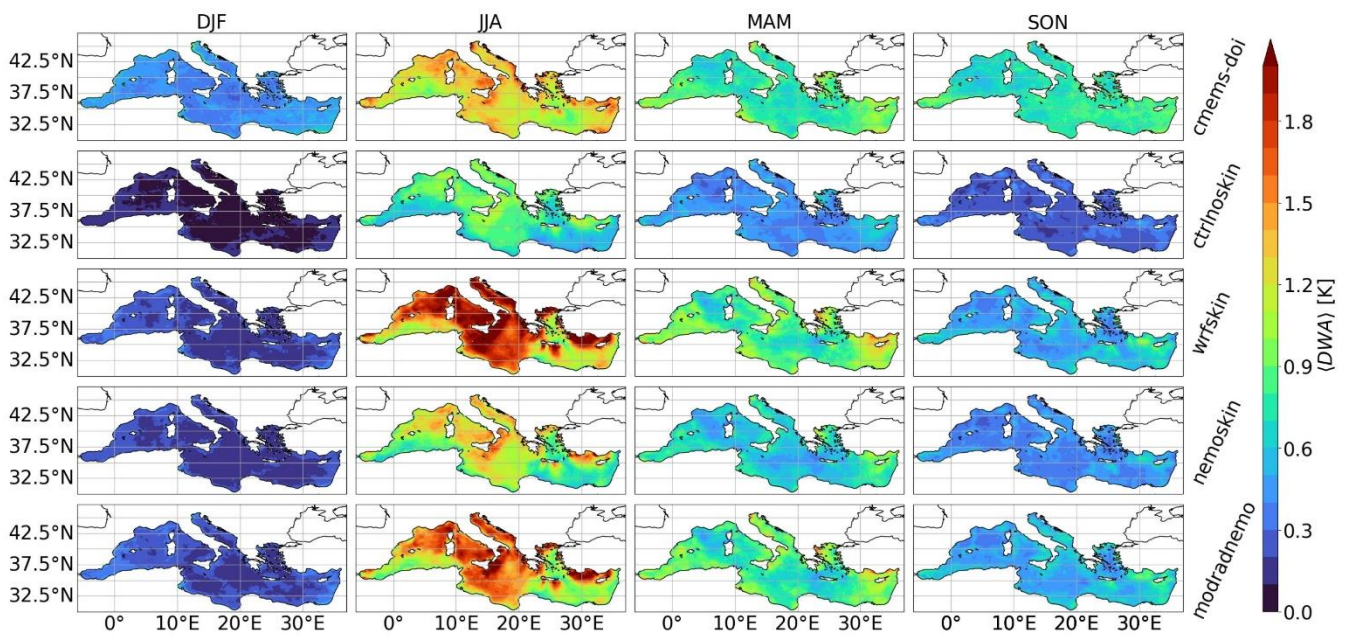
Figure 4: Mean diurnal warming amplitude averaged over seasons (on columns), for each case (row): the first row is the CMEMS MED DOISST data, followed in order by the control simulation, wrfskin, nemoskwrite and modradnemo.

581

582

583
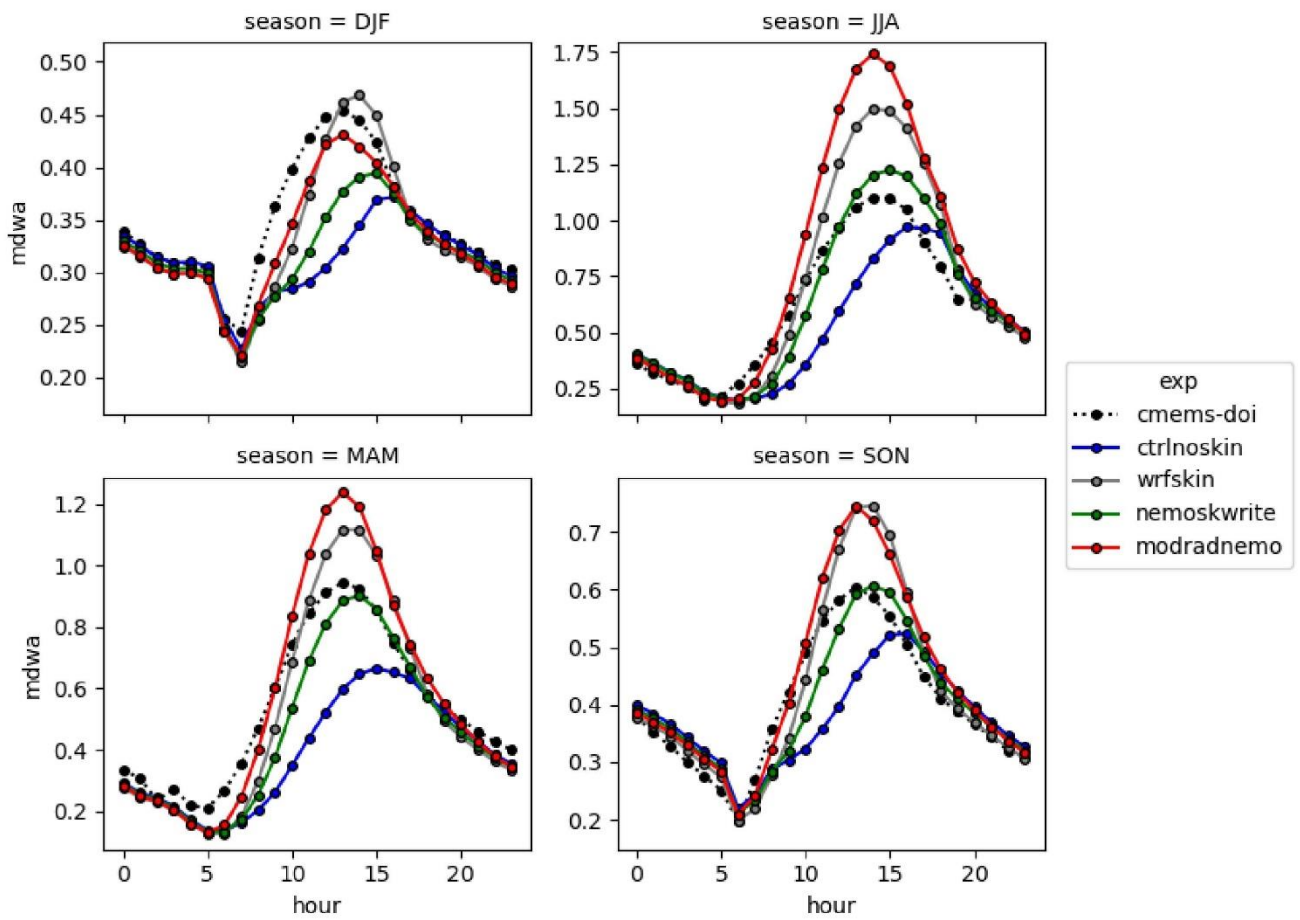
584

585 **Figure 5**: Seasonality of the diurnal cycle averaged over the whole Mediterranean Sea, masking out regions in
586 time and space where the percentage of model data in CMEMSDOI is greater than 50%.
587
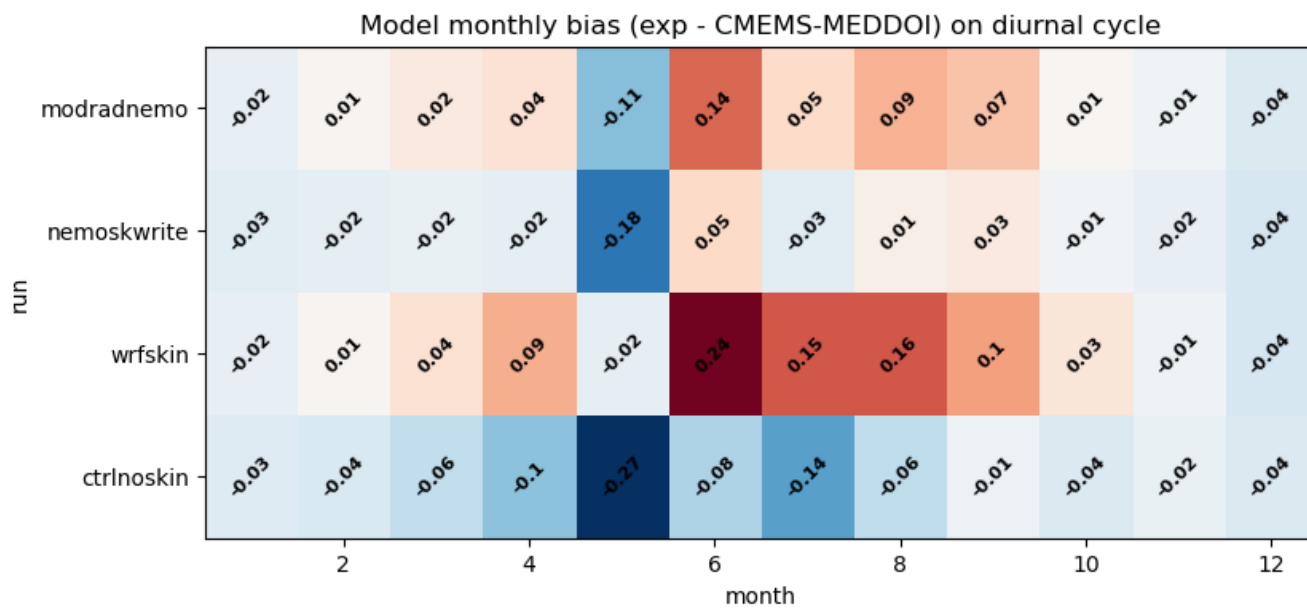
Figure 6: Monthly averaged values for the time series of spatial mean diurnal cycle over the Mediterranean Sea (bias with respect to CMEMS MED DOISST)

593
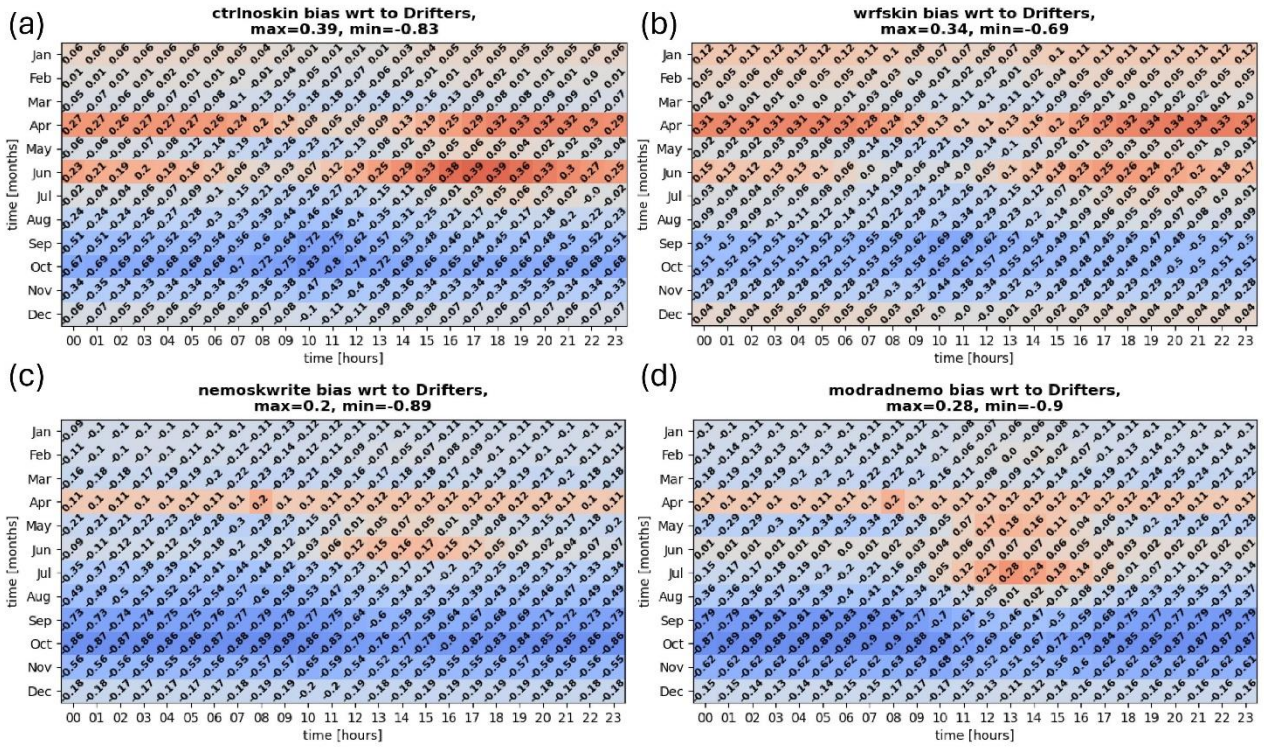
594
595 **Figure 7**: Bias with respect to measurements averaged over drifters' locations as a function of the month and
596 the time of the day. Panels 7a, 7b, 7c, 7d show respectively the results for all the simulations carried out in the
597 present study. Confidence on these numbers can be supported by the numbers of measurements reported in table
598 S1.
599

600

601
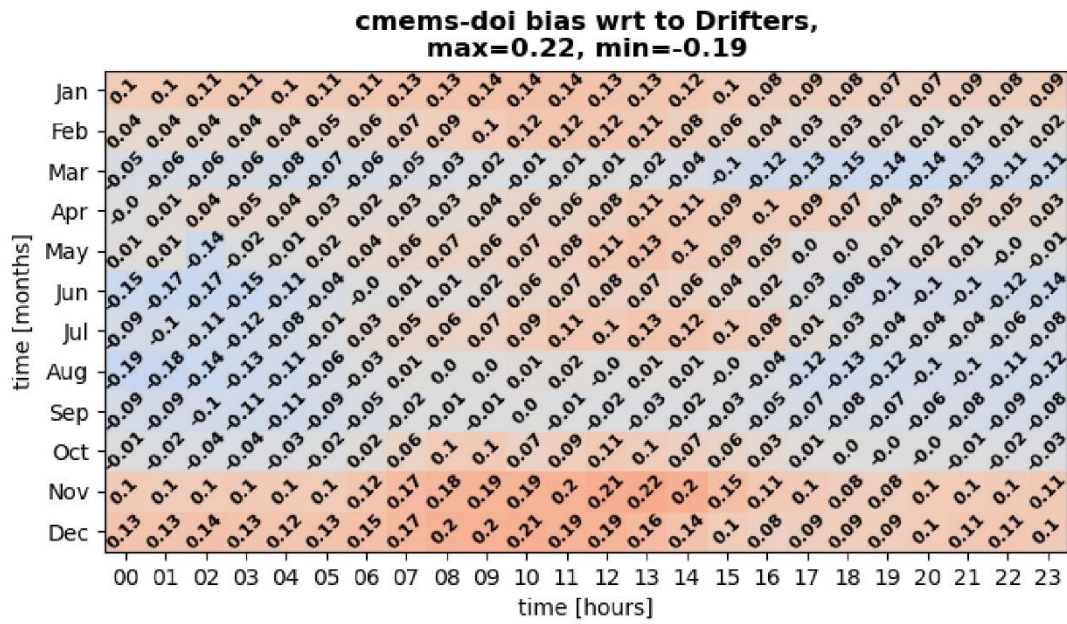
602

603 **Figure 8**: Bias with respect to measurements averaged over drifters' locations as a function of the month and
604 time of the day, for CMEMS MED DOISST data.
605
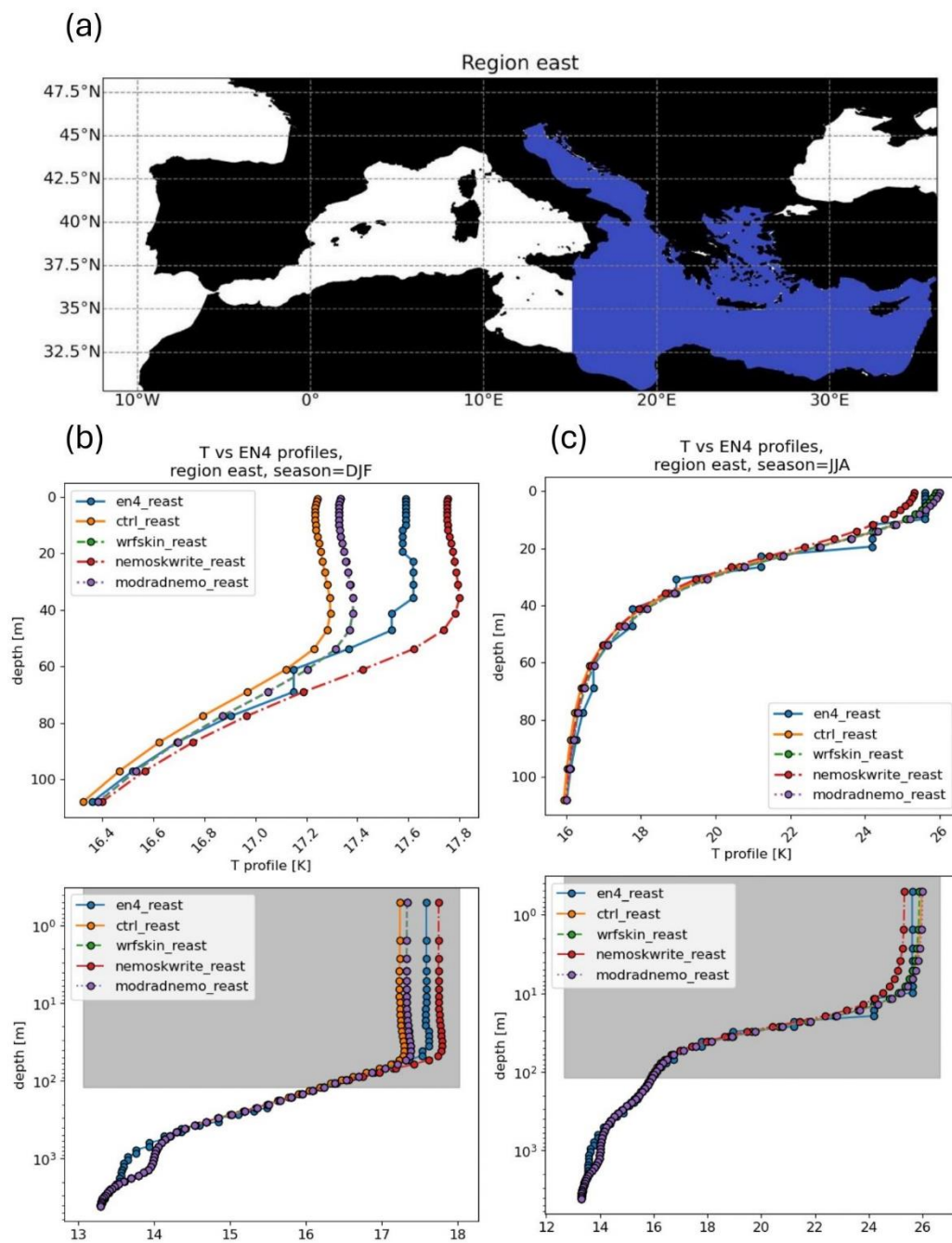
607
Figure 9: Spatial average of profiles within the eastern Mediterranean Sea, during winter and summer. Panel
9a shows the eastern region, while 9b, 9c show respectively wintertime and summertime spatially averaged
profiles within the top 100 *m* in the upper part, on the bottom the whole depth range on a logarithmic scale.
611

612
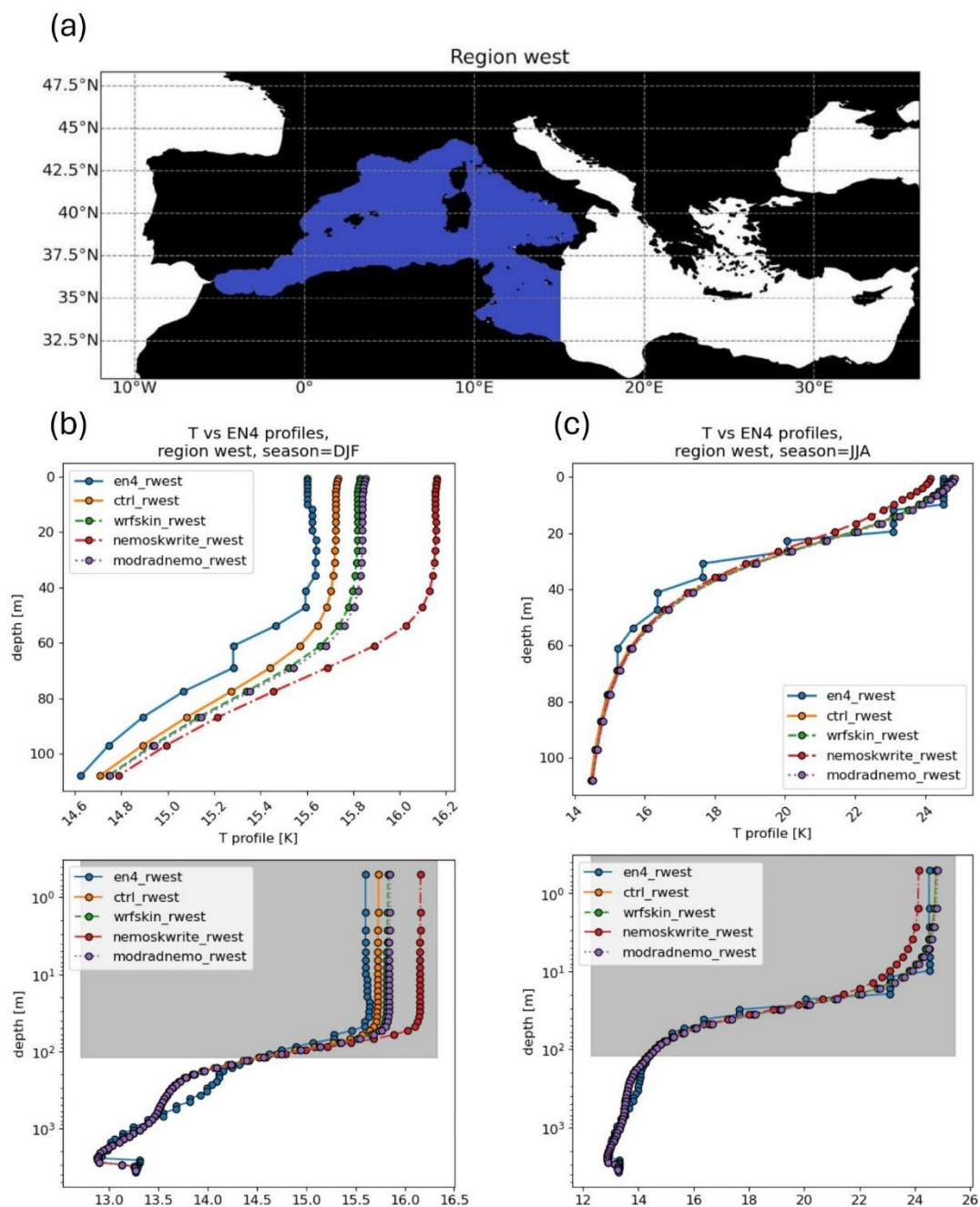
613
Figure 10: Spatial average of profiles within the eastern Mediterranean Sea, during winter and summer. Panel
10a shows the eastern region, while 10b, 10c show respectively wintertime and summertime spatially-averaged
profiles within the top 100 *m* in the upper part, on the bottom the whole depth range on a logarithmic scale.
617
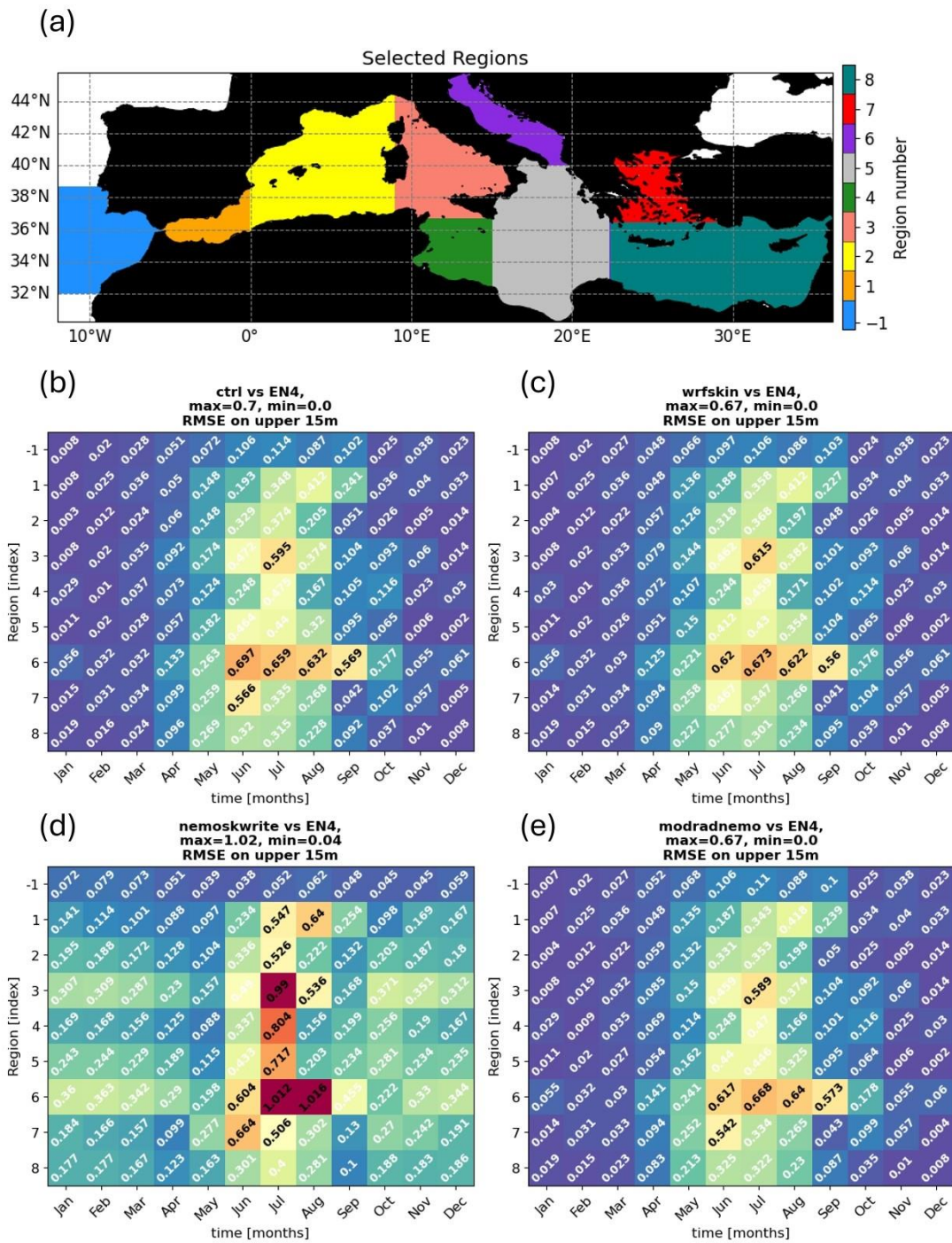
Figure 11: RMSE on the top 15m of the difference between regionally averaged profiles between each simulation and EN4, displayed as a function of the region and the particular month. Division in regions is reported in panel 11a, while 11b, 11c, 11d, 10e show respectively the results for all the simulations carried out in the present study.
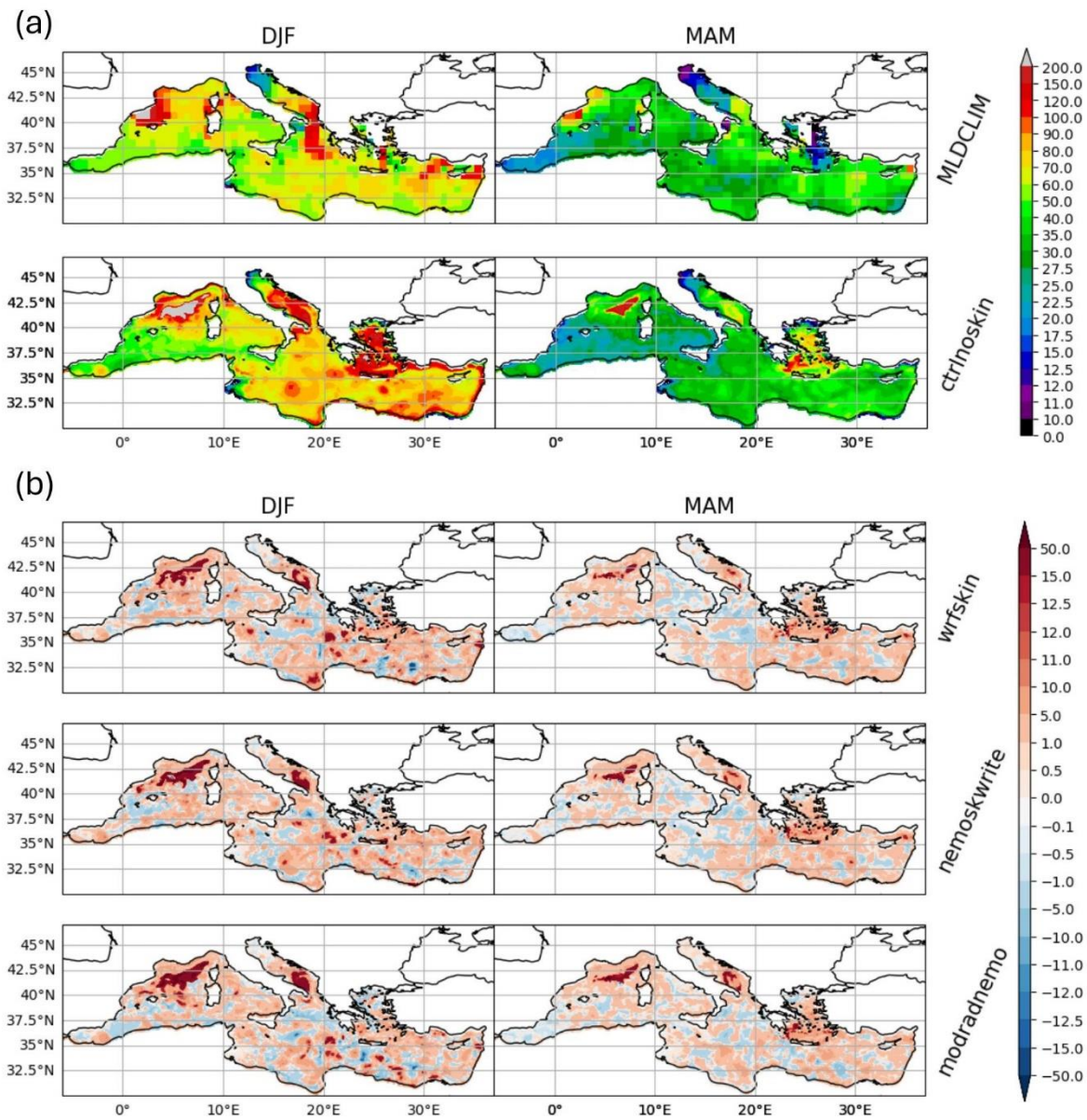
Figure 12: Maps of DJF, MAM of mixed layer depth for the climatology and for the control simulation in panel (a). Panel (b) shows the difference of the control with respect to each simulation. Units are meters.

624
625
626
627
628

629
630
631
632
633
634
635
636
637
638
639
640
641
642
643

644

645
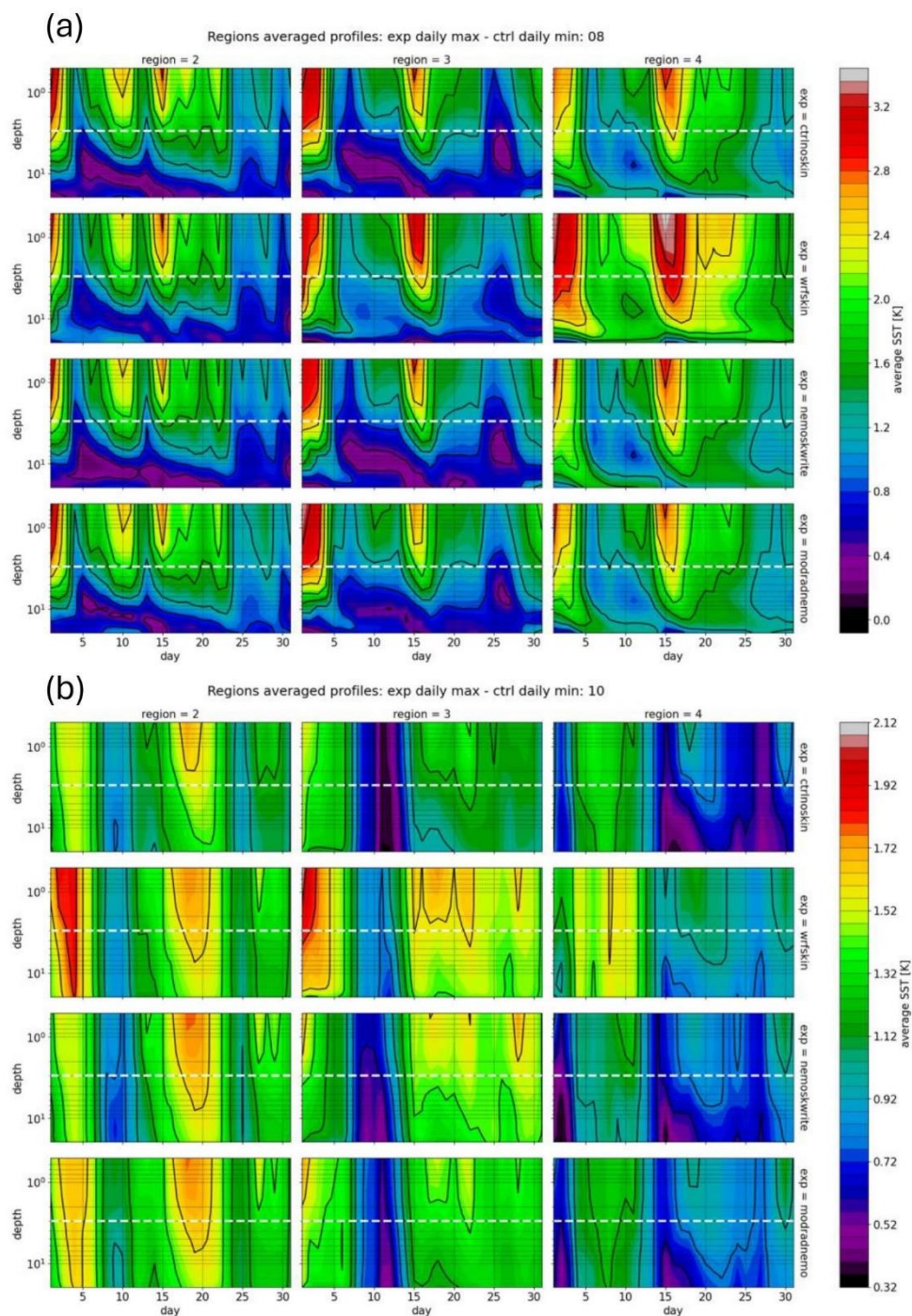
Figure 13: Hovmoller plots for spatial average of model outputs temperature profiles in the regions 2,3,4 as defined by figure 11a. Each row shows the difference between daily maxima for the given experiment minus the daily minima for the control simulation. The white dashed line traces the $z = 3m$ line of the depth used as reference for the base of the warm layer as in ZB05 scheme Zeng and Beljaars, 2005. Panel 13a shows August, panel 13b shows October.

651

652

Tables

653

654

Simulation	Scheme active	Extinction coefficients in Warm Layer
ctrlnoskin	None	None
wrfskin	ZB05	SS82
nemoskwrite	ZB05+A02+T10	G09
modradnemo	ZB05+A02+T10	R-G-B + chl e-folding

655   **Table 1**: Overview of the simulations performed

656

Wavelength $[\mu m]$	i	a_i	$b_i \; [m^{-1}]$
0.3-0.6	1	0.2370	1.488×10^{-1}
0.6-0.9	2	0.3600	4.405×10^{-1}
0.9-1.2	3	0.1790	3.175×10^{1}
1.2-1.5	4	0.0870	1.825×10^{2}
1.5-1.8	5	0.0800	1.201×10^{3}
1.8-2.1	6	0.0246	7.937×10^{3}
2.1-2.4	7	0.0250	3.195×10^{3}
2.4-2.7	8	0.0070	1.279×10^{4}
2.7-3.0	9	0.0004	6.944×10^{4}

657   **Table 2**: Parameters for the Transmission coefficient following Soloviev and Schlüssel, 1996, in which the
658   first coefficients is the average between the one corresponding to I, IA, IB, II, and III Jerlov optical water types.
659   This is currently implemented in NEMO.

simulation	DJF	MAM	JJA	SON	Annual
ctrlnoskin	-173.31	133.92	75.56	-66.40	-7.55
wrfskin	-168.83	134.19	76.51	-65.87	-5.97
nemoskwrite	-169.28	133.79	76.77	-65.72	-6.10
modradnemo	-169.06	134.87	78.16	-68.13	-6.04
ERA5	-140.36	133.24	81.96	-53.46	5.35

Table 3: Averaged surface net heat flux over the Mediterranean Sea (W/m^2): seasonal and annual spatial averaged mean values.

References

Artale, V., Iudicone, D., Santoleri, R., Rupolo, V., Marullo, S., and d'Ortenzio, F.: Role of surface fluxes in ocean general circulation models using satellite Sea Surface Temperature: Validation of and sensitivity to the forcing frequency of the Mediterranean thermohaline circulation. *Journal of Geophysical Research: Oceans*, 107(C8):29–1, 2002.

Bernie, D., Guilyardi, E., Madec, G., Slingo, J., and Woolnough, S.: Impact of resolving the diurnal cycle in an ocean–atmosphere GCM. Part 1: A diurnally forced OGCM. *Climate Dynamics*, 29:575–590, 2007.

Bernie, D., Guilyardi, E., Madec, G., Slingo, J. M., Woolnough, S. J., and Cole, J.: Impact of resolving the diurnal cycle in an ocean–atmosphere GCM. Part 2: A diurnally coupled C-GCM. *Climate dynamics*, 31:909–925, 2008.

Chen, S. S. and Houze Jr, R. A.: Diurnal variation and life-cycle of deep convective systems over the tropical pacific warm pool. *Quarterly Journal of the Royal Meteorological Society*, 123(538):357–388, 1997.

Craig, A., Valcke, S., and Coquart, L.: Development and performance of a new version of the OASIS coupler, OASIS3-MCT 3.0. *Geoscientific Model Development*, 10(9):3297– 3308, 2017.

Criado-Aldeanueva, F., Soto-Navarro, F. J., & García-Lafuente, J.: Seasonal and interannual variability of surface heat and freshwater fluxes in the Mediterranean Sea: Budgets and exchange through the Strait of Gibraltar. *International Journal of Climatology*, 32(2), 286-302, 2012.

Vincenzo de Toma. (2024). Skin Sea Surface Temperature schemes in coupled ocean-atmosphere modeling: the impact of chlorophyll-interactive e-folding depth. Intermediate results and scripts to produce the figures. Zenodo. https://doi.org/10.5281/zenodo.10818183

Donlon, C., Robinson, I., Casey, K., Vazquez-Cuervo, J., Armstrong, E., Arino, O., Gentemann, C., May, D., LeBorgne, P., Piollé, J., et al.: The global ocean data assimilation experiment high-resolution Sea Surface Temperature pilot project. *Bulletin of the American Meteorological Society*, 88(8):1197–1214, 2007.

Fairall, C., Bradley, E. F., Godfrey, J., Wick, G., Edson, J. B., and Young, G.: Cool-skin and warm-layer effects on Sea Surface Temperature. *Journal of Geophysical Research: Oceans*, 101(C1):1295–1308, 1996.

Gentemann, C. L., Minnett, P. J., and Ward, B.: Profiles of ocean surface heating (POSH): A new model of upper ocean diurnal warming. *Journal of Geophysical Research: Oceans*, 114(C7), 2009.

Gonzalez, N. M.: Multi-scale modelling of Gibraltar Straits and its regulating role of the Mediterranean climate (*Doctoral dissertation, Université Paul Sabatier-Toulouse III*), 2023.

Gouretski, V. and Cheng, L.: Correction for systematic errors in the global dataset of temperature profiles from mechanical bathythermographs. *Journal of Atmospheric and Oceanic Technology*, 37(5):841–855, 2020.

Gouretski, V. and Reseghetti, F.: On depth and temperature biases in bathythermograph data: Development of a new correction scheme based on analysis of a global ocean database. *Deep Sea Research Part I: Oceanographic Research Papers*, 57(6):812– 833, 2010.

Hagemann, S., Stacke, T., & Ho-Hagemann, H. T.: High resolution discharge simulations over Europe and the Baltic Sea catchment. *Frontiers in Earth Science*, 8, 12, 2020.

Hersbach, H., Bell, B., Berrisford, P., Hirahara, S., Horányi, A., Muñoz-Sabater, J., Nicolas, J., Peubey, C., Radu, R., Schepers, D., et al.: The ERA5 global reanalysis. *Quarterly Journal of the Royal Meteorological Society*, 146(730):1999–2049, 2020.

Houpert L, Testor P, Durrieu de Madron X.: Gridded climatology of the Mixed Layer (Depth and Temperature), the bottom of the Seasonal Thermocline (Depth and Temperature), and the upper-ocean Heat Storage Rate for the Mediterrean Sea. SEANOE. https://doi.org/10.17882/46532, 2015a.

Houpert, L., Testor, P., De Madron, X. D., Somot, S., D'ortenzio, F., Estournel, C., & Lavigne, H.: Seasonal cycle of the mixed layer, the seasonal thermocline and the upper-ocean heat storage rate in the Mediterranean Sea derived from observations. Progress in Oceanography, 132, 333-352, 2015b.

Jansen, E., Pimentel, S., Tse, W. H., Denaxa, D., Korres, G., Mirouze, I., & Storto, A.: Using canonical correlation analysis to produce dynamically based and highly efficient statistical observation operators. Ocean Science, 15(4), 1023-1032, 2019.

Jerlov, N. G.: Optical Oceanography. Amsterdam, London and New York: Elsevier Publishing Co, 1968.

Jordà, G., Von Schuckmann, K., Josey, S. A., Caniaux, G., García-Lafuente, J., Sammartino, S., ... & Macías, D.: The Mediterranean Sea heat and mass budgets: Estimates, uncertainties and perspectives. *Progress in Oceanography*, 156, 174-208, 2017.

Karagali, I. and Høyer, J.: Observations and modeling of the diurnal SST cycle in the North and Baltic seas. *Journal of Geophysical Research: Oceans*, 118(9):4488–4503, 2013.

Kawai, Y. and Wada, A.: Diurnal Sea Surface Temperature variation and its impact on the atmosphere and ocean: A review. *Journal of oceanography*, 63:721–744, 2007.

Large, W. G., McWilliams, J. C., and Doney, S. C.: Oceanic vertical mixing: A review and a model with a nonlocal boundary layer parameterization. *Reviews of geophysics*, 32(4):363–403, 1994.

Lee, Z., Du, K., Arnone, R., Liew, S., & Penta, B. (2005). Penetration of solar radiation in the upper ocean: A numerical model for oceanic and coastal waters. *Journal of Geophysical Research: Oceans*, 110(C9).

Lengaigne, M., Menkes, C., Aumont, O., Gorgues, T., Bopp, L., André, J. M., & Madec, G.: Influence of the oceanic biology on the tropical Pacific climate in a coupled general circulation model. Climate Dynamics, 28, 503-516, 2007.

Leonelli, F. E., Bellacicco, M., Pitarch, J., Organelli, E., Buongiorno Nardelli, B., De Toma, V., ... & Santoleri, R. (2022). Ultra-oligotrophic waters expansion in the North Atlantic Subtropical Gyre revealed by 21 years of satellite observations. *Geophysical Research Letters*, 49(21), e2021GL096965.

Macdonald, A. M., Candela, J., & Bryden, H. L.: An estimate of the net heat transport through the Strait of Gibraltar. *Seasonal and Interannual Variability of the Western Mediterranean Sea*, 46, 13-32, 1994.

Marullo, S., Pitarch, J., Bellacicco, M., Sarra, A. G. d., Meloni, D., Monteleone, F., Sferlazzo, D., Artale, V., and Santoleri, R.: Air–sea interaction in the central Mediterranean Sea: Assessment of reanalysis and satellite observations. *Remote Sensing*, 13(11):2188, 2021.

Marullo, S., Santoleri, R., Banzon, V., Evans, R. H., & Guarracino, M.: A diurnal-cycle resolving sea surface temperature product for the tropical Atlantic. Journal of Geophysical Research: Oceans, 115(C5), 2010.

Marullo, S., Minnett, P. J., Santoleri, R., & Tonani, M.: The diurnal cycle of sea-surface temperature and estimation of the heat budget of the Mediterranean S ea. Journal of Geophysical Research: Oceans, 121(11), 8351-8367, 2016.

Minnett, P., Alvera-Azc´arate, A., Chin, T., Corlett, G., Gentemann, C., Karagali, I., Li, X., Marsouin, A., Marullo, S., Maturi, E., et al.: Half a century of satellite remote sensing of Sea Surface Temperature. *Remote Sensing of Environment*, 233:111366, 2019.

Morel, A., & Antoine, D. (1994). Heating rate within the upper ocean in relation to its bio–optical state. *Journal of Physical Oceanography*, 24(7), 1652-1665.

Morel, A., & Berthon, J. F.: Surface pigments, algal biomass profiles, and potential production of the euphotic layer: Relationships reinvestigated in view of remote-sensing applications. Limnology and oceanography, 34(8), 1545-1562, 1989.

NEMO System Team: *NEMO ocean engine*, 1288-1619 (isnn) edition, 2019.

Ohlmann, J. C., Siegel, D. A., & Mobley, C. D. (2000). Ocean radiant heating. Part I: Optical influences. *Journal of Physical Oceanography*, 30(8), 1833-1848.

Ohlmann, J. C., & Siegel, D. A. (2000). Ocean radiant heating. Part II: Parameterizing solar radiation transmission through the upper ocean. *Journal of Physical Oceanography*, 30(8), 1849-1865.

Penny, S. G., Akella, S., Balmaseda, M. A., Browne, P., Carton, J. A., Chevallier, M., Counillon, F., Domingues, C., Frolov, S., Heimbach, P., et al.: Observational needs for improving ocean and coupled reanalysis, S2S prediction, and decadal prediction. *Frontiers in Marine Science*, 6:391, 2019.

Pettenuzzo, D., Large, W. G., & Pinardi, N.: On the corrections of ERA-40 surface flux products consistent with the Mediterranean heat and water budgets and the connection between basin surface total heat flux and NAO. *Journal of Geophysical Research: Oceans*, 115(C6), 2010.

Pisano, A., Ciani, D., Marullo, S., Santoleri, R., and Buongiorno Nardelli, B.: A new operational mediterranean diurnal optimally interpolated SST product within the copernicus marine environment 2 monitoring service 3. *Earth System Science Data Discussions*, 2022:1–26, 2022.

Ruiz, S., Gomis, D., Sotillo, M. G., & Josey, S. A.: Characterization of surface heat fluxes in the Mediterranean Sea from a 44-year high-resolution atmospheric data set. *Global and Planetary Change*, 63(2-3), 258-274, 2008.

Saunders, P. M.: The temperature at the ocean-air interface. *Journal of Atmospheric Sciences*, 24(3):269–273, 1967.

Skamarock, W. C., Klemp, J. B., Dudhia, J., Gill, D. O., Liu, Z., Berner, J., Wang, W., Powers, J. G., Duda, M. G., Barker, D. M., et al.: A description of the advanced research WRF model version 4. *National Center for Atmospheric Research: Boulder, CO, USA*, 145(145):550, 2019.

Soloviev, A.: On the vertical structure of the ocean thin surface layer at light wind. *Dokl. Acad. Sci. USSR, Earth Sci. Serr*, pages 751–760, 1982.

Soloviev, A. and Lukas, R.: Observation of large diurnal warming events in the near-surface layer of the western equatorial pacific warm pool. *Deep Sea Research Part I: Oceanographic Research Papers*, 44(6):1055–1076, 1997.

Soloviev, A. and Lukas, R.: The near-surface layer of the ocean: structure, dynamics and applications, *volume 48. Springer Science & Business Media*, 2013.

Soloviev, A. V. and Schlussel, P.: Evolution of cool skin and direct air-sea gas transfer coefficient during daytime. *Boundary-Layer Meteorology*, 77(1):45–68, 1996.

Song, X. and Yu, L.: Air-sea heat flux climatologies in the Mediterranean Sea: Surface energy balance and its consistency with ocean heat storage. *Journal of Geophysical Research: Oceans*, 122(5):4068–4087, 2017.

Storto, A., Alvera-Azcárate, A., Balmaseda, M. A., Barth, A., Chevallier, M., Counillon, F., ... & Zuo, H.: Ocean reanalyses: recent advances and unsolved challenges. Frontiers in Marine Science, 6, 418, 2019.

Storto, A. and Oddo, P.: Optimal assimilation of daytime SST retrievals from SEVIRI in a regional ocean prediction system. *Remote Sensing*, 11(23):2776, 2019.

789 Storto, A., Hesham Essa, Y., de Toma, V., Anav, A., Sannino, G., Santoleri, R., & Yang, C.: MESMAR v1: A
790   new regional coupled climate model for downscaling, predictability, and data assimilation studies in the
791   Mediterranean region. Geoscientific Model Development Discussions, 2023, 1-40, 2023.

793 Takaya, Y., Bidlot, J.-R., Beljaars, A. C., and Janssen, P. A.: Refinements to a prognostic scheme of skin Sea
794   Surface Temperature. *Journal of Geophysical Research: Oceans*, 115(C6), 2010.

795 Tu, C.-Y. and Tsuang, B.-J.: Cool-skin simulation by a one-column ocean model. *Geophysical research letters*,
796   32(22), 2005.

797 Valdivieso, M., Haines, K., Balmaseda, M., Chang, Y. S., Drevillon, M., Ferry, N., ... & Andrew Peterson, K.:
798   An assessment of air–sea heat fluxes from ocean and coupled reanalyses. *Climate Dynamics*, 49, 983-1008,
799   2017.

800 Volpe, G., Colella, S., Brando, V. E., Forneris, V., La Padula, F., Di Cicco, A., Sammartino, M., Bracaglia, M.,
801   Artuso, F., and Santoleri, R.: Mediterranean ocean colour level 3 operational / multi-sensor processing. *Ocean
802   Science*, 15(1):127–146, 2019.

803 Ward, B.: Near-surface ocean temperature. *Journal of Geophysical Research: Oceans*, 111(C2), 2006.

804 While, J., Mao, C., Martin, M., Roberts-Jones, J., Sykes, P., Good, S., and McLaren, A.: An operational analysis
805   system for the global diurnal cycle of Sea Surface Temperature: implementation and validation. *Quarterly
806   Journal of the Royal Meteorological Society*, 143(705):1787–1803, 2017.

807 Xu, F. and Ignatov, A.: In situ SST quality monitor (i-quam). *Journal of Atmospheric and Oceanic Technology*,
808   31(1):164–180, 2014.

809 Zeng, X. and Beljaars, A.: A prognostic scheme of sea surface skin temperature for modeling and data
810   assimilation. *Geophysical Research Letters*, 32(14), 2005.

812 Zhang, R., Zhou, F., Wang, X., Wang, D., & Gulev, S. K.: Cool skin effect and its impact on the computation
813   of the latent heat flux in the South China Sea. *Journal of Geophysical Research: Oceans*, *126*(1),
814   2020JC016498, 2021.

816 Zuo, H., Balmaseda, M. A., Mogensen, K., & Tietsche, S.: OCEAN5: the ECMWF ocean reanalysis
817   system and its real-time analysis component (p. 44). Reading, UK: European Centre for Medium-
818   Range Weather Forecasts, 2018.